Journal of Oncology Research and Therapy
Loshusan BR, et al. Oncol Res Ther 9: 10198.
www.doi.org/10.29011/2574-710X.10198
www.gavinpublishers.com

OPEN ACCESS

GAVIN PUBLISHERS

Research article

Young's Moduli of Human Lung Parenchyma and Tumours

Brandon R Loshusan[1], Arefin M Shamsil[2,5], Michael D Naish[2,3,4,5], Rajni V Patel[2,4,5,6], Mehdi Qiabi[6,7], Rahul Nayak[6,7], Richard A Malthaner[5,6,7*]

[1]Schulich School of Medicine & Dentistry, Western University, London, Ontario, Canada

[2]School of Biomedical Engineering, Western University, London, Ontario, Canada

[3]Department of Mechanical and Materials Engineering, Western University, London, Ontario, Canada [4]Department of Electrical and Computer Engineering, Western University, London, Ontario, Canada

[5]Canadian Surgical Technologies & Advanced Robotics, London Health Sciences Centre, London, Ontario, Canada

[6]Department of Surgery, Schulich School of Medicine & Dentistry, London, Ontario, Canada

[7]Division of Thoracic Surgery, London Health Sciences Centre, London, Ontario, Canada

Corresponding author: Richard Malthaner, Canadian Surgical Technologies & Advanced Robotics, London Health Sciences Centre, London, Ontario, Canada

Citation: Loshusan BR, Shamsil AM, Naish MD, Patel RV, Qiabi M, et al. (2024) Young's Moduli of Human Lung Parenchyma and Tumours. J Oncol Res Ther 9: 10198. DOI: 10.29011/2574-710X.10198

Received Date: 23 January, 2024; **Accepted Date:** 30 January, 2024; **Published Date**: 2 February, 2024

Abstract

Tumour localization of small deep subpleural lesions during VATS depends on the differential tissue stiffness between a tumour and the adjacent tissue. To obtain a quantitative measure of stiffness, we catalogued the Young's Modulus of *in situ* abnormal lung lesions and adjacent tissue from resected specimens.

A 5 to 10 mm section of resected tumour and adjacent lung tissue was placed in a custom indenting elastometer device to measure the Young's Modulus. The device applied a uniform force on the tissue samples to varying levels of tissue displacement — up to 15% of their thickness. The Young's Modulus was calculated from 200 measurements of forces and displacements. Each set of measurements was repeated three times. The Young's Modulus for each tissue histology was assessed by parametric or nonparametric analyses as appropriate.

The median [range] Young's Modulus for all lung tumours (12.73 kPa [2.68–199.10]; $p < 0.001$) was significantly higher than adjacent lung tissue (6.12 kPa [1.65–13.19]; $p < 0.001$). Adenocarcinomas, squamous cell carcinomas, various metastases, and granuloma/fibromas had Young's Modulus values greater than adjacent lung histologies.

This is the first study to report the elastic properties of human lung parenchyma in various disease states and abnormal lesions. There was a significant difference between the Young's Moduli of human lung tumours and parenchyma. These findings may aid in the development of improved intraoperative localization technologies for minimally invasive pulmonary surgeries.

Introduction

Lung cancer is the leading cause of death from cancer for both men and women in Canada [1]. Screening for lung cancer and safe surgical resection is the most promising strategy to improve lung cancer survival [2,3]. The preferred method of lung cancer resection is by Video Assisted Thoracic Surgery (VATS); however, VATS can make it difficult for the surgeon to accurately identify small and deep subpleural nodules. When this occurs, the surgeon must make a larger thoracotomy to manually palpate and locate these subpleural nodules. Avoiding the need to intraoperatively transition to an open thoracotomy is preferable for improved patient outcomes [4].

We have developed a Tactile-Sensing System ("finger on a stick" lung palpator) that is wireless and provides visual feedback to identify deep subpleural lung nodules [5–7]. Our current lab phantom tumour model consists of silicon and agar-based spheres that have excellent acoustic properties for detection by ultrasound but lack the appropriate elastic properties needed for the tactile imaging experiments. Better *ex vivo* and *in vivo* phantom models of lung tumours are needed [5,6,8].

The standard surgical practice of palpation is based on the qualitative assessment of the stiffness of tissue. The Young's Modulus (YM) can be used to define the stiffness of tissue and is expressed as the relationship between stress and strain of a material. It is calculated from the slope of the stress–strain curve and can be achieved by compressing a sample of tissue by a controlled amount while measuring the resulting forces. This value has been discussed in the context of breast cancer and colorectal cancer, but not for human lung tumours or in healthy lung tissue [9,10]. While this information is relevant on its own, it would also allow for the development of more accurate tumour models that can help translate tactile imaging technology to the operating room to detect subpleural lung nodules.

The purpose of this study was to assess the YM quantitative values of lung nodules in select patients with suspected lung cancer. We hypothesized that there would be a difference between the YM of lung tumours and normal lung parenchyma. We believed that there may be a correlation between the YM and different histological tissues in human lung (adenocarcinoma, squamous cell carcinoma, normal lung tissue), with an expected range of YM for each tumour type.

Patients and Methods

We examined the YM of a cohort of patients presenting with clinical and radiographic evidence of lung nodules that underwent surgical resection at Victoria Hospital, London Health Sciences Centre, London, Ontario, Canada. Participants were excluded if they were younger than 18 years of age or were unable to provide informed consent. Patients with suspected metastatic disease, and previous neoadjuvant therapy were included. All patients underwent either a VATS or thoracotomy resection of the tumour by a board-certified thoracic surgeon. Immediately following surgical resection, a 5–10-millimeter section of tumour and a similar-sized sample of healthy adjacent lung tissue were removed from the resected specimen.

To measure the YM of tissue, our team constructed a portable indenting device (Figure 1). The device measured the YM using two different modalities per test. The first method applied a unform force over a small surface area on lung tissue samples such that the tissue was compressed by 15% of its thickness. The device measured the force applied and displacement of the tissue 200 times during the procedure. We defined the results of this process as the "linear YM". The device then performed an indentation test using the second technique. The indenter compressed the tissue to its maximum strain level and allowed the tissue to return to its original thickness at a rate of 10 Hz. The force applied and displacement of the tissue were measured 200 times. This was repeated for 20 cycles to yield a total of 4000 data points. We defined the results of this process as the "cyclic YM". Each iteration of the test yielded one linear and cyclic YM result. These measurements were repeated three times for each lung nodule and adjacent lung sample.

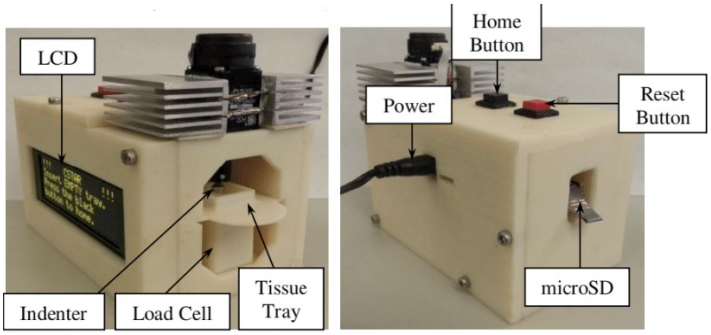

Figure 1: Labelled image of the tissue indentation device used to measure the Young's Modulus.

The displacement and force data collected were converted to microns and micro-Newtons respectively and saved on a microSD card. The YM was calculated according to the equation below:

$$E = \frac{3}{\pi^2 R} \frac{(n\sum_{i=1}^{n} W_i F_i - \sum_{i=1}^{n} W_i \sum_{i=1}^{n} F_i)}{(n\sum_{i=1}^{n} W_i^2 - (\sum_{i=1}^{n} W_i)^2)}$$

where E is the YM, n is the number of data points, R is the radius of the indenter tip, F is the applied force, and W is the displacement of the indenter. The coefficient term corrects for the size of the indenter tip [11]. The tissue displacement and force measurement accuracies were within 30–50 microns and 0.2–0.4 micronewtons, respectively.

The size of the tumour, Positron Emission Tomography (PET) Maximum Specific Uptake Value (SUV Max), histological diagnosis, location, and neoadjuvant chemotherapy/radiation, as well as the patient's age and sex were recorded and stored in our REDCap database to maintain patient privacy and confidentiality. Data analysis was performed using Microsoft Excel Version 16.69.1 and XLSTAT Premium Version 24.3.1. The average cyclic and linear YM was calculated based on the results from each test. Pearson Product Moment correlation and Spearman's Rank correlation tests were performed to assess the associations between the clinical and pathological variables and measured YM. The results were considered significant if $R > 0.70$. The frequency distribution of the YM of each tissue histology was assessed for normality using the Shapiro-Wilk test. For nonparametric data, the Mann-Whitney U-test was used to compare the differences in YM for each histology. A threshold p value of 0.05 was used to assess for statistical significance.

Results

The normality of each distribution was assessed by using the Shapiro-Wilk test at a significance level of a=0.05. The null hypothesis of this test stated that the sample was taken from a normal distribution. As displayed in Table 1, the computed p-values were lower than the significance level. Therefore, we did not accept the null hypothesis and the Mann-Whitney U-test was used for our analyses. The linear and cyclic YM results follow a similar distribution and have negligible differences in measurement results for tumour or adjacent lung tissue. Thus, we reported the linear YM results for our analysis. Tumour and adjacent lung YM measurements were compared in different subsets based on the histology of tumour. The complete results of our analysis are displayed in Table 2. On aggregate, the median linear YM for lung tumours (12.73 kPa [2.68–199.10]; $p < 0.001$) was statistically greater than adjacent lung tissue (6.12 kPa [1.65–13.19]; $p < 0.001$) as seen in Table 3 and Figure 2. The median linear YM for adenocarcinomas (12.51 kPa [2.68–199.10]; $p < 0.001$) was statistically greater than adjacent lung tissue (6.24 kPa [1.65–13.19]; $p < 0.001$) as displayed in Table 3 and Figure 3. The median linear YM for squamous cell carcinoma (12.88 kPa [5.03–73.96]; $p < 0.001$) was statistically greater than adjacent lung tissue (6.13 kPa [4.13–9.58]; $p < 0.001$) described in Table 3 and Figure 4. The various metastatic tumours included colorectal carcinoma, breast carcinoma, adenoid cystic carcinoma, renal cell carcinoma, and melanoma. All metastases were grouped together due to the small sample size of each individual pathological subset. The median linear YM for lung metastases (12.57 kPa [7.40–73.96]; $p < 0.001$) was statistically greater than for adjacent lung tissue (5.14 kPa [3.28–10.19]; $p < 0.001$) as seen in Table 3 and Figure 5. For adjacent lung tissue, there were no statistically significant differences in the median YM of healthy lung tissue and fibrotic lung tissue, emphysematous changes, or other various benign pathologies. The median YM values were stratified based on the grade of lung tumours and were not statistically significantly different. For both pathological T-stage and N-stage, there were no statistically significant differences between the median YM values of lung tumours. When considering tumour location, there was no statistically significant difference between median YM values for lung tumours.

The Pearson Product Moment Correlation test was performed between the linear YM and the following variables: patient age; patient sex; the number of cigarette packs (20 cigarettes/pack) smoked per day multiplied by the number of years smoked (smoking pack-years); PET SUV Max; size of lesion on Computed Tomography (CT); and size of lesion from histology. We found no significant correlation between the average linear YM values and these variables since they all had an $R < 0.70$.

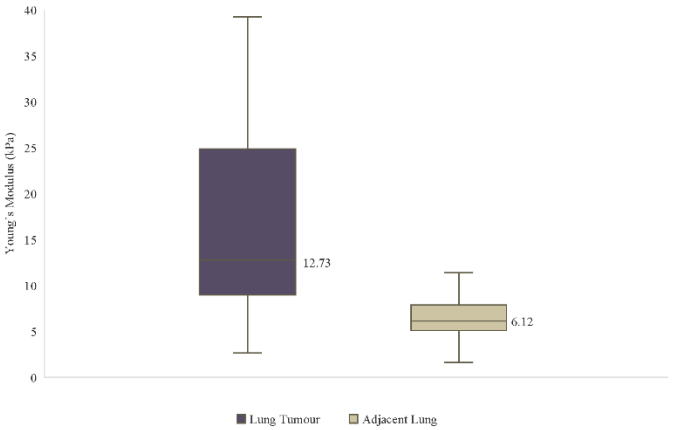

Figure 2: Standard box plots of the median and interquartile range of the Young's Modulus of all lung tumours compared to adjacent lung tissue.

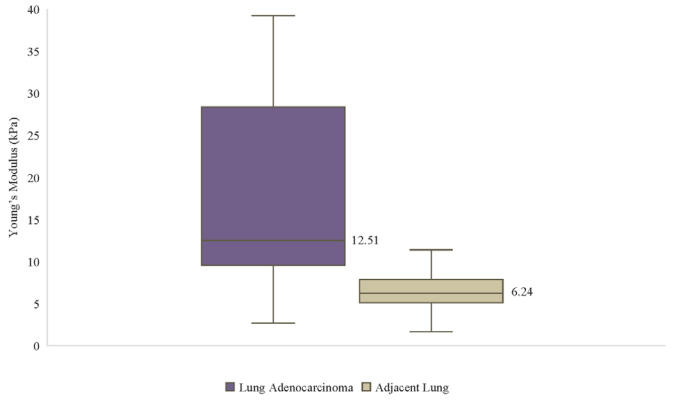

Figure 3: Standard box plots of the median and interquartile range of the Young's Modulus of adenocarcinomas compared to adjacent lung tissue.

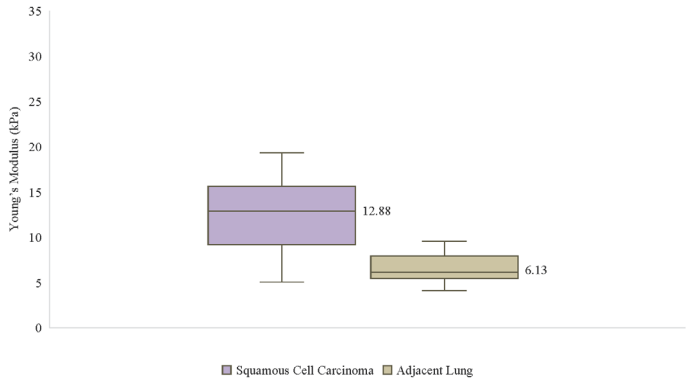

Figure 4: Standard box plots of the median and interquartile range of the Young's Modulus of squamous cell carcinomas compared to adjacent lung tissue.

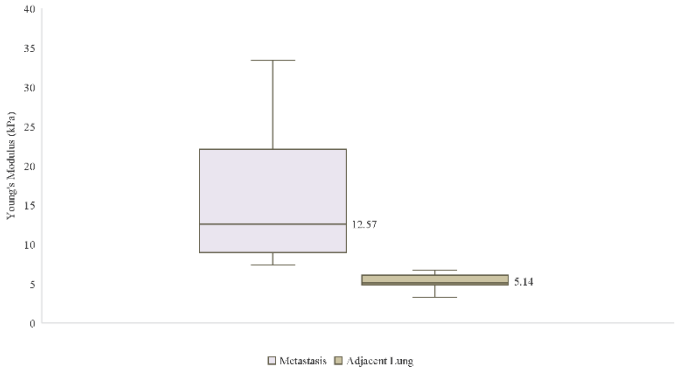

Figure 5: Standard box plots of the median and interquartile range of the Young's Modulus of various metastases compared to adjacent lung tissue.

Measurement	Median Young's Modulus (kPa)	Range (kPa)	P value
Linear YM—Tumour (*n* = 78)	12.73	2.68–199.10	< .001
Cyclic YM—Tumour (*n* = 78)	15.24	3.97–191.32	< .001
Linear YM—Adjacent Lung (*n* = 78)	6.54	1.65–13.19	.03
Cyclic YM—Adjacent Lung (*n* = 78)	9.41	2.03–15.32	.45

Table 1: Median linear vs. cyclic Young's Modulus for tumour and adjacent ling tissue and Shapiro Wilk test results for normality.

	Median Young's Modulus (kPa)	Range (kPa)	P value
Total			
Lung Tumour (*n* = 78)	12.73	2.68–199.10	< .001
Adjacent Lung (*n* = 78)	6.12	1.65–13.19	< .001
Lung Tumour			

Adenocarcinoma (*n* = 39)	12.51	2.68–199.10	< .001
Squamous Cell Carcinoma (*n* = 17)	12.88	5.03–73.96	< .001
Adenosquamous Carcinoma (*n* = 3)	29.70	10.48–154.90	.10
[a]Other (*n* = 4)	6.47	4.36–10.14	.89
Metastasis			
CRC, BR, ACC, RCC, M (*n* = 11)	12.57	7.40–73.96	< .001
Benign Nodule			
Granulomas and Fibromas (*n* = 4)	17.59	13.26–52.11	.03
Adjacent Lung			
Healthy Lung (*n* = 60)	6.09	1.65–13.19	—
Fibrosis (*n* = 5)	6.72	4.13–8.59	.99
Emphysematous Changes (*n* = 10)	5.82	3.66–10.29	.98
[b]Other (*n* = 3)	8.24	6.11–8.36	.23
Tumour Grade			
GX (*n* = 19)	13.26	4.46–73.96	—
G1 (*n* = 6)	16.96	3.62–66.32	.78
G2 (*n* = 28)	12.69	2.68–199.10	.75
G3 (*n* = 23)	10.92	4.01–80.34	.50
G4 (*n* = 2)	12.11	7.46–16.76	.61
Pathologic T-stage			
T1b (*n* = 11)	11.96	2.68–154.90	—
T1c (*n* = 12)	13.26	3.62–35.08	.74
T2a (*n* = 20)	12.89	5.03–199.10	.38
T2b (*n* = 8)	29.25	8.17–73.96	.18
T3 (*n* = 11)	13.13	4.01–80.34	.85
T4 (*n* = 5)	10.60	4.46–33.41	.91
Not applicable (*n* = 11)	13.26	7.40–73.96	.40
Pathologic N-stage			
NX (*n* = 9)	17.54	6.24–154.92	—
N0 (*n* = 43)	12.88	2.68–199.10	.34
N1 (*n* = 12)	8.05	3.62–35.54	.03
N2 (*n* = 3)	12.51	11.19–73.95	.86
Not applicable (*n* = 11)	13.26	7.40–73.96	.50
Tumour Location			
Right Upper Lobe (*n* = 29)	13.26	4.01–73.96	—
Right Middle Lobe (*n* = 3)	11.79	10.92–20.14	.81

Right Lower Lobe (*n* = 10)	11.74	2.68–154.90	.95
Left Upper Lobe (*n* = 18)	15.81	3.62–199.10	.87
Left Lower Lobe (*n* = 18)	11.91	5.03–80.34	.32

[a]Other = Small cell lung carcinoma, large cell lung cancer, carcinoid/ neuroendocrine tumours

[b]Other = granulomatous inflammation, lipoid pneumonia, inflammation

Abbreviations:

ACC: adenoid cystic carcinoma; BR, breast; CRC, colorectal carcinoma; M: melanoma

RCC: renal cell carcinoma.

Table 2: Comparison of median linear Young's Modulus values based on tumour and adjacent normal lung histology.

	Median YM (kPa)	Range (kPa)	P value
Total			
Lung Tumour (*n* = 78)	12.73	2.68 - 199.10	< .001
Normal Adjacent Lung (*n* = 78)	6.12	1.65 - 13.19	< .001
Lung Tumour			
Adenocarcinoma (*n* = 39)	12.51	2.68 - 199.10	< .001
Adjacent Lung (*n* = 39)	6.24	1.65 - 13.19	< .001
Squamous Cell Carcinoma (*n* = 17)	12.88	5.03 - 73.96	< .001
Adjacent Lung (*n* = 17)	6.13	4.13 - 9.58	< .001
Metastasis			
CRC, BR, ACC, RCC, M (*n* = 11)	12.57	7.40 - 73.96	< .001
Adjacent Lung (*n* = 11)	5.14	3.28 - 10.19	< .001
Benign Nodule			
Granulomas and Fibromas (*n* = 4)	17.59	13.26 - 52.11	.03
Adjacent Lung (*n* = 4)	9.71	8.24 - 10.29	.03

Table 3: Summary of median Young's Modulus tumour measurements that were statistically significant compared to adjacent normal lung.

Comment

This study presents the first measurements of the YM of lung tumours and adjacent lung tissue for various pathologies. The measurements were obtained by indentation testing of recent surgically excised lung tumours and adjacent lung tissue. The YM of biological tissue can be estimated through various indirect methods, such as ultrasound, shear wave elastography, or harmonic motion elastography. These indirect methods use imaging techniques to noninvasively mimic palpation below the skin's surface to determine the YM of tissues. However, the YM values obtained from these non-invasive techniques are only estimates that are qualitative in nature. Our indentation device, based on the work of Egorov *et al.*, has been specifically designed to measure the YM of small tissue samples and produces repeatable quantitative measurement [11].

Measuring the YM of various biological tissues to gain a better understanding of sinister pathologies is not a novel concept. In fact, there are several studies that aim to characterize the YM in breast tissue, colorectal tissue, bladder tumours, oropharyngeal structures, and even dog lungs [12–16]. Some studies have attempted to estimate the YM of human lungs using transthoracic shear wave ultrasound. Early work by Liu *et al.* points to transthoracic shear wave elastography as being efficacious in differentiating between benign and malignant lung lesions [17]. However, later work by Quarto *et al*. concludes that the clinical utility of shear wave elastography in the lung is limited by factors such as fat or air [18]. The lack of repeatable outcomes in this method of measuring the YM of lung tumours and lung parenchyma presents a gap in the literature. Our study aimed to fill this gap by directly measuring the YM via indentation

Both the linear and cyclic YM measurements from our device displayed repeatable results and a statistically significant agreement with one another. The results of the linear YM testing showed a statistically significant difference in median YM values between lung tumours and adjacent lung tissue. Similar results were obtained for the median YM for lung adenocarcinoma; squamous cell carcinoma; and various lung metastases which were all found to be greater than adjacent lung tissue. These results are consistent with other cancers that typically display a substantially higher YM than normal biological tissue [10]. For lung cancers, this could potentially be due to the significant smoking history of the participants, which could result in emphysematous lung tissue. Although we did not find a significant correlation between the number of smoking pack years and the YM of tumours, research has shown that smoking causes a significant increase in the stiffness of cadaveric lung tissue in smokers versus nonsmokers [19]. Furthermore, researchers have found differences in the YM of healthy and damaged lung tissue in murine models at the cellular level [20]. Increased cellular turn over and dysplasia could result in the stiffening of normal lung tissue and lung tumours.

We found no significant relationship or difference between the YM of lung tumours and patient sex, age, smoking pack years, tumour grade, location, CT size, SUV Max, pathological T-stage, or N-stage. This contrasts the finding that the YM of colorectal cancer tissue correlates with pathological tumour size and venous invasion [21]. Our results may reflect the small sample size tested in these subgroups. Further research should attempt to recruit a larger number of participants to derive statistically significant correlations between the YM of lung tumours and clinical variables.

Our contributions to the existing body of literature are twofold. This is the first time that the YM of human lung cancers and healthy lung tissue from recent surgical specimens have been directly measured by indentation testing. Secondly, this is the first study to assess the relationship between the YM of human lung cancers and histopathological variables. These results may allow us to develop more realistic phantom tumour models to improve minimally invasive surgical techniques.

In conclusion, there is a statistically significant difference between the YM of lung parenchyma and tumours. These differences are apparent in histologies such as adenocarcinomas, squamous cell carcinomas, and various lung metastases.

Acknowledgements

The authors would like to thank the thoracic surgeons, anesthesiologists, operating room nurses and research coordinators for their support. The authors would also like to thank Jochem van Gaalen for designing and building the tissue indentation device used in this study and the Lawson Health Research Institute for making this research possible.

Disclosures

Conflict of Interest: The authors declare no conflict of interest.

Ethics Statement: The study protocol was approved by the Western University Health Sciences Research Ethics Board (REB# 112607) and conformed to the tenets of the Declaration of Helsinki.

References

1. Cancer Care Ontario. Ontario Cancer Statistics 2022, Chapter 2: Estimated Current Cancer Mortality.
2. Lewin G, Morissette K, Dickinson J, et al. (2016) Recommendations on screening for lung cancer. CMAJ 188: 425–432.
3. Aberle DR, Adams AM, Berg CD, et al. (2011) Reduced lung-cancer mortality with low-dose computed tomographic screening. N Engl J Med 365: 1533–4406.
4. Bendixen M, Jorgensen OD, Kronborg C, Andersen C, Licht PB (2016) Postoperative pain and quality of life after lobectomy via video-assisted thoracoscopic surgery or anterolateral thoracotomy for early-stage lung cancer: a randomised controlled trial. Lancet Oncol 17: 1474–5488.
5. McCreery GL, Trejos AL, Naish MD, Patel RV, Malthaner RA (2008) Feasibility of locating tumours in lung via kinaesthetic feedback. Int J Med Robotics and Computer Assisted Surgery 4: 58–68.
6. Perri MT, Trejos AL, Naish MD, Patel RV, Malthaner RA (2010) New tactile sensing system for minimally invasive surgical tumour localization. Int J Med Robot 6: 211–220.
7. Naidu AS, Escoto A, Fahmy O, Patel RV, Naish MD (2016) An autoclavable wireless palpation instrument for minimally invasive surgery. Paper presented at: 38th Annual International Conference of the IEEE Engineering in Medicine and Biology Society (EMBC); Orlando, FL.
8. Escoto A, Bhattad S, Shamsil A, et al. (2015) A multi-sensory mechatronic device for localizing tumors in minimally invasive interventions. Paper presented at: IEEE International Conference on Robotics and Automation (ICRA); Seattle, WA.
9. Kawano S, Kojima M, Higuchi Y, et al. (2015) Assessment of elasticity of colorectal cancer tissue, clinical utility, pathologic and phenotypical relevance. Cancer Sci 106: 1232–1239.

10. Samani A, Zubovits J, Plewes D (2007) Elastic moduli of normal and pathological human breast tissues: an inversion-technique-based investigation of 169 samples. Phys Med Biol 52: 1565–1576.

11. Egorov V, Tsyuryupa S, Kanilo S, Kogit M, Sarvazyan A (2008) Soft tissue elastometer. Med Eng Phys 30: 206–212.

12. McKee CT, Last JA, Russell P, Murphy CJ (2011) Indentation versus tensile measurements of Young's Modulus for soft biological tissues. Tissue Eng 17: 155–164.

13. Samani A, Plewes D (2004) A Method to measure the hypereleastic parameters of ex vivo breast tissue samples. Phys Med Biol 49: 4395–4405.

14. Haddad SMH, Dhaliwal SS, Rotenberg BW, Ladak HM, Samani A (2020) Estimation of the hyperelastic parameters of fresh human oropharyngeal soft tissues using indentation testing. J Mech Behav Biomed Mater 108: 1–9.

15. Lee JW, Lorenzo EIS, Ahn B, et al. (2011) Palpation device for the identification of kidney and bladder cancer: a pilot study. Yonsei Med J 52: 768–772.

16. Lai-Fook SJ, Wilson TA, Hyatt RE, Rodarte JR (1976) Elastic constants of inflated lobes of dog lungs. J Appl Physiol 40: 508–513.

17. Liu Y, Zhen Y, Zhang X, Gao F, Lu X (2021) Application of transthoracic shear wave elastography in evaluating subpleural pulmonary lesions. Eur J Radiol Open 8: 1–6.

18. Quarto CMI, Venuti M, Dimitri L, et al. (2022) Transthoracic ultrasound shear wave elastography for the study of subpleural lung lesions. Ultrasonography 41: 93–105.

19. Karimi A, Razaghi R (2018) The role of smoking on the mechanical properties of the human lung. Technol Health Care 26: 963–972.

20. Chen J, Mir SM, Pinezich MR, et al. (2021) Non-destructive vacuum-assisted measurement of lung elastic modulus. Acta Biomater 16: 36–47.

21. Kawano S, Kojima M, Higuchi Y, et al. (2015) Assessment of elasticity of colorectal cancer tissue, clinical utility, pathological and phenotypical relevance. Cancer Sci 106: 1232–1239.